ESTIMATING LARGE LOCAL MOTION IN LIVE-CELL IMAGING USING VARIATIONAL OPTICAL FLOW

Towards Motion Tracking in Live Cell Imaging Using Optical Flow

Jan Hubený, Vladimír Ulman and Pavel Matula
Centre for Biomedical Image Analysis, Faculty of Informatics Masaryk University, Botanická 68a, Brno 602 00, Czech Republic

Keywords: Live-cell imaging, motion tracking, 3D imaging, variational optical flow.

Abstract: The paper studies the application of state-of-the-art variational optical flow methods for motion tracking of fluorescently labeled targets in living cells. Four variants of variational optical flow methods suitable for this task are briefly described and evaluated in terms of the average angular error. Artificial ground-truth image sequences were generated for the purpose of this evaluation. The aim was to compare the ability of those methods to estimate local divergent motion and their suitability for data with combined global and local motion. Parametric studies were performed in order to find the most suitable parameter adjustment. It is shown that a selected optimally tuned method tested on real 3D input data produced satisfactory results. Finally, it is shown that by using appropriate numerical solution, reasonable computational times can be achieved even for 3D image sequences.

1 INTRODUCTION

There is a steadily growing interest in live cell studies in modern cell biology. The progress in staining of living cells together with advances in confocal microscopy devices has allowed detailed studies of the behaviour of intracellular components including the structures inside the cell nucleus. The typical number of investigated cells in one study varies from tens to hundreds because of statistical significance of the results. One gets time-lapse series of three or two dimensional images as an output from the microscope. It is very inconvenient and annoying to analyze such data sets by hand (especially for 3D series). Moreover, there is no guarantee on the accuracy of the results. Therefore, there is a natural demand for computer vision methods which can help with analysis of these time-lapse image series. Estimation or correction of *global* as well as *local* motion belongs to main tasks in this field. The suitability of the state-of-the-art optical flow methods for correction of *local* motion will be studied in this article.

The live-cell studies are mainly performed using the confocal microscopes these days. The confocal microscopes are able to focus on selected z-plane of the specimen in the same way as the standard wide-field (non-confocal) microscopes. However, they are based on principle of suppression of light from planes which are out of focus. Therefore, they provide far better 3D image data (less blurred) than wide-field microscopes. The main disadvantage of confocal microscopes is their lower light throughput. This causes larger exposure times as compared to the wide-field mode. Several optical setups suitable for live-cell imaging as well as their optimization and automation are discussed in detail in (Kozubek et al., 2004).

Transparent biological material is visualized with fluorescent proteins in live-cell imaging. Living specimen usually does not contain fluorescent proteins. Therefore, the living cells are forced to produce those proteins in the specimen preparation phase (Chalfie et al., 1994). The image of the living cells in the specimen on the microscope stage is acquired periodically. The cells can move or change their internal structure in the meantime. The interval between two consecutive acquisitions varies in range from fractions of second up to tens of minutes. It would be convenient to acquire snapshots frequently in order to have only small changes between two consecutive frames. But, the interval length cannot be arbitrary

Hubený J., Ulman V. and Matula P. (2007).
ESTIMATING LARGE LOCAL MOTION IN LIVE-CELL IMAGING USING VARIATIONAL OPTICAL FLOW - Towards Motion Tracking in Live Cell Imaging Using Optical Flow.
In *Proceedings of the Second International Conference on Computer Vision Theory and Applications - IU/MTSV*, pages 542-548
Copyright © SciTePress

small mainly because of photo-toxicity (the living specimen is harmed by the light) and photo-bleaching (the intensity of fluorescent markers fades while being exposed to the light). However, it is usually possible to find a reasonable compromise between those restrictions and adjust the image acquisition so that the displacement of objects between two consecutive snapshots is not more than ten pixels.

There are two types of tasks to be solved in this field. First, the *global* movement of objects should be corrected before subsequent analysis of an intracellular movement. This goal is often achieved using common rigid registration methods (Zitová and Flusser, 2003). A fast 3D point based registration method (Matula et al., 2006) was recently proposed for the global alignment of cells.

The second task is to estimate *local* changes inside the objects. This task is more complex. The objects inside the cells or nuclei can move in different directions. One object can split into two or more objects and vice versa. Moreover, an object can appear or disappear during the experiment. Therefore, this task requires computation of dense motion field between two consecutive snapshots. Manders et. al. has used block-matching (BM3D) algorithm (de Leeuw and van Liere, 2002) for this purpose in their study of chromatin dynamics during the assembly of interphase nuclei (Manders et al., 2003). Their BM3D algorithm is rather slow. It is similar to basic optic flow methods but it does not comprise any smoothness term.

We study latest optical flow methods (Bruhn, 2006) for estimation of intracellular movement in this paper. Up to our best knowledge, nobody investigated the application of these state-of-the-art methods in live-cell imaging. The simple ancestors of these methods, which can reliably estimate one pixel motion, were successfully used for lung motion correction (Dawood et al., 2005). The examined methods are able to reliably estimate the flow larger than one pixel. They can produce piece-wise smooth flow fields which preserve the discontinuities in the flow on object boundaries. These properties are needed for estimation of *local* divergent motion which occur in live-cell imaging. We have extended state-of-the-art optical flow methods into three dimensions. Especially, we focused on 3D extension of recently published optical flow methods for large displacements (Papenberg et al., 2006). We tested these methods on synthetic as well as real data and compared their behaviour and performance. Our experiments identify the optical flow methods which can be used in live cell imaging. We used the efficient numeric techniques for the optical flow computations (Bruhn, 2006). This allows us to get reasonable computational times even for 3D image sequences.

The rest of the paper is organized as follows: The variational optical flow methods are described in Section 2. Section 3 is devoted to the experiments and results obtained for synthetic and real biomedical data.

2 OPTICAL FLOW

In this section, we describe the basic ideas of variational optical flow methods and in particular the methods which will be tested in Section 3.

Let two consecutive frames of image sequence be given. Optical flow methods compute the displacement vector field which maps all voxels from first frame to their new position in the second frame. Although several kinds of strategies exist for optical flow computation (Barron et al., 1994), we take only the so-called variational optical flow (VOF) methods into our considerations. They currently give the best results (in terms of error measures) (Papenberg et al., 2006; Bruhn and Weickert, 2005) and come out from transparent mathematical modeling (the flow field is described by energy functional). Furthermore, they produce dense flow fields and are invariant under rotations.

The first prototype of VOF method was proposed in (Horn and Schunck, 1981). Horn and Schunck used the grey value constancy assumption which assumes that the grey value intensity of the moving objects remains the same and homogenous regularization which assumes that the flow is smooth. We will describe their method first, because even the most sophisticated methods available are based on the fundamental ideas of Horn and Schunck method.

Let $\Omega_4 \subset \mathbb{R}^4$ denote the 4-dimensional spatial-temporal image domain and $f(x_1,\dots,x_4) : \Omega_4 \to \mathbb{R}$ a gray-scale image sequence, where $(x_1,x_2,x_3)^\top$ is a voxel location within a image domain $\Omega_3 \subset \mathbb{R}^3$ and $x_4 \in [0,T]$ denotes the time. Moreover, let's assume that $\Delta x_4 = 1$ and $\mathbf{u} = (u_1,u_2,u_3,1)^\top$ denotes the unknown flow. The grey value constancy assumption says

$$f(x_1+u_1,\dots,x_3+u_3,x_4+1) - f(x_1,\dots,x_4) = 0 \quad (1)$$

Optic flow constraint (OFC) is obtained by approximation of (1) with first-order Taylor expansion

$$f_{x_1}u_1 + f_{x_2}u_2 + f_{x_3}u_3 + f_{x_4} = 0, \qquad (2)$$

where f_{x_i} is partial derivative of f. Equation (2) with three unknowns has obviously more than one solution. Horn and Schunck assumed only smooth flows and they therefore penalized the solutions which have

large spatial gradient $\nabla_3 u_i$ where $i \in 1,2,3$ and ∇_3 denotes the spatial gradient. Thus, the sum $\sum_{i=1}^{3} |\nabla_3 u_i|$ for every voxel should be as small as possible. We get following variational formulation of the problem if we combine these two considerations together:

$$E_{\mathrm{HS}}(\mathbf{u}) = \int_{\Omega} (f_{x_1} u_1 + f_{x_2} u_2 + f_{x_3} u_3 + f_{x_4})^2 + \alpha \sum_{i=1}^{3} |\nabla_3 u_i|^2 d\mathbf{x} \tag{3}$$

The optimal displacement vector field minimizes energy functional (3). The OFC and the regularizer are squared, the α parameter has the influence on the smoothness of the solution. The two terms which form the functional are called *data* and *smoothness* term. Following the calculus of variations (Gelfand and Fomin, 2000), the minimizer of (3) is a solution of Euler-Lagrange equations

$$\begin{aligned} 0 &= f_{x_1}^2 u_1 + f_{x_1} f_{x_2} u_2 + f_{x_1} f_{x_3} u_3 + f_{x_1} f_{x_4} + \alpha \operatorname{div}(\nabla_3 u_1) \\ 0 &= f_{x_1} f_{x_2} u_1 + f_{x_2}^2 u_2 + f_{x_2} f_{x_3} u_3 + f_{x_2} f_{x_4} + \alpha \operatorname{div}(\nabla_3 u_2) \\ 0 &= f_{x_1} f_{x_3} u_1 + f_{x_2} f_{x_3} u_2 + f_{x_3}^2 u_3 + f_{x_3} f_{x_4} + \alpha \operatorname{div}(\nabla_3 u_3) \end{aligned} \tag{4}$$

with reflecting Neumann boundary conditions. $\operatorname{div}(\mathbf{x})$ is the divergence operator. The system (4) is usually solved with common numerical methods like Gauss-Seidel or SOR. The bidirectional full multigrid (Briggs et al., 2000) framework for computations of VOF methods was proposed in (Bruhn et al., 2005). The computations with multigrid methods are by orders of magnitude faster than the classic Gauss-Seidel or SOR methods.

Now we describe the VOF methods which will be tested in Section 3. The current state-of-the-art VOF methods are still similar to their Horn-Schunck precursor. Their energy functional consists of *data* and *smoothness* term. The combined local-global (CLG) method for large displacements proposed in (Papenberg et al., 2006) is the first method which we have tested. This method produces one among the most accurate results (Bruhn, 2006). We assume that it will be suitable for our data, because it produces smooth flow fields and simultaneously flow fields with discontinuities. The energy functional of CLG method is defined as:

$$E_{\mathrm{CLG}}(\mathbf{u}) = \int_{\Omega} \Psi_{\mathrm{D}}(|f(\mathbf{x}+\mathbf{u}) - f(\mathbf{x})|^2) + \alpha \Psi_{\mathrm{S}} \left(\sum_{i=1}^{3} |\nabla_3 u_i|^2 \right) d\mathbf{x} \tag{5}$$

where

$$\Psi_{\mathrm{D}}(s) = \sqrt{s^2 + \varepsilon_{\mathrm{D}}^2} \quad \Psi_{\mathrm{S}}(s) = \sqrt{s^2 + \varepsilon_{\mathrm{S}}^2}$$

and ε_{D}, ε_{S} are reasonably small numbers (e.g. $\varepsilon_{\mathrm{D}} = 0.01$). Note that the data term consists of *non-linearized* grey value constancy assumption (1). This allows to correct estimate of the large displacements. Moreover, the CLG method uses the non-quadratic penalizers $\Psi_{\mathrm{D}}(s)$ and $\Psi_{\mathrm{S}}(s)$ and therefore it is robust with respect to noise and outliers. Nevertheless, these concepts make the minimization of (5) quite complex. We use the multi-scale warping based approach, which proposed in (Papenberg et al., 2006), for minimization of (5). The multigrid numerical framework for this task was extensively analyzed in (Bruhn, 2006; Bruhn and Weickert, 2005).

The second tested method consists of robust data term and anisotropic image driven smoothness term (Nagel and Enkelmann, 1986). We denote this method RDIA. Its energy functional is defined:

$$E_{\mathrm{RDIA}}(\mathbf{u}) = \int_{\Omega} \Psi_{\mathrm{D}}(|f(\mathbf{x}+\mathbf{u}) - f(\mathbf{x})|^2) + \alpha \sum_{i=1}^{3} (\nabla_3 u_i^{\top} P_{\mathrm{NE}}(\nabla_3 f) \nabla_3 u_i)\, d\mathbf{x} \tag{6}$$

where $P_{\mathrm{NE}}(\nabla_3 f)$ is projection matrix perpendicular to $\nabla_3 f$ defined as

$$P_{\mathrm{NE}} = \frac{1}{2|\nabla_3 f|^2 + 3\varepsilon^2} \begin{pmatrix} a & b & c \\ b & d & e \\ c & e & f \end{pmatrix} \tag{7}$$

where

$$\begin{aligned} a &= f_{x_2}^2 + f_{x_3}^2 + \varepsilon^2 & d &= f_{x_1}^2 + f_{x_3}^2 + \varepsilon^2 \\ b &= -f_{x_1} f_{x_2} & e &= -f_{x_2} f_{x_3} \\ c &= -f_{x_1} f_{x_3} & f &= f_{x_1}^2 + f_{x_2}^2 + \varepsilon^2 \end{aligned}$$

The ε is reasonably small number (e.g. $\varepsilon = 0.01$). The only difference between CLG and RDIA method is the smoothing term. RDIA method smoothes the flow with respect to underlying image. The image data in live-cell imaging are often low contrast due to the limitations of the optical setup. We assume that this smoothing term can help with processing of such data. The same minimization approach can be used as for the CLG method.

The third and fourth tested method are variants of the previous two. We add the gradient constancy assumption to the data term. This should provide us better results on image sequences which fade out with increasing time. The energy functional of CLG method

with gradient constancy assumption is defined as

$$E_{\mathrm{CLG_G}}(\mathbf{u}) = \int_\Omega \Psi_{\mathrm{D}}(|f(\mathbf{x}+\mathbf{u}) - f(\mathbf{x})|^2 + \gamma(|\nabla f(\mathbf{x}+\mathbf{u}) - \nabla f(\mathbf{x})|^2)) + \alpha\Psi_{\mathrm{S}}\left(\sum_{i=1}^{3}|\nabla_3 u_i|^2\right) d\mathbf{x} \tag{8}$$

The variant of RDIA method with gradient constancy assumption is defined as

$$E_{\mathrm{RDIA_G}}(\mathbf{u}) = \int_\Omega \Psi_{\mathrm{D}}(|f(\mathbf{x}+\mathbf{u}) - f(\mathbf{x})|^2 + \gamma(|\nabla f(\mathbf{x}+\mathbf{u}) - \nabla f(\mathbf{x})|^2)) + \alpha\sum_{i=1}^{3}(\nabla_3 u_i^\top P_{\mathrm{NE}}(\nabla_3 f)\nabla_3 u_i)\, d\mathbf{x} \tag{9}$$

where γ is the parameter which controls the influence of gradient constancy assumption. Note that the gradient constancy assumption is again included in the non-linearized form.

3 RESULTS AND DISCUSSION

In this section, we test the behaviour of CLG, RDIA, $\mathrm{CLG_G}$ and $\mathrm{RDIA_G}$ methods on artificial and real image data. We measure their performance on live-cell image sequences with large local displacements. Moreover, we present the results of the methods on image sequences with combined global rigid (translation, rotation) and local displacements. We present the results on both two and three dimensional data. Finally, we discuss the computational time and storage demands.

The ground-truth flow fields are needed for the evaluation purposes. Obviously, they are not available for real image sequences. Therefore, we generate the artificial data with artificial flow fields from the real image data. We use the two-layered approach in which user-selected foreground is locally moved and inserted into an artificially generated background. Hence, our generator requires one real input frame, the mask of the cell (the background) and the mask of the objects (the foreground). Both first and second frames are generated in two steps. First, the foreground objects are extracted, an artificial background is generated and the rigid motion is applied on background and foreground separately. Second, every foreground object is translated independently on each other and finally inserted into the generated background. The movements were performed by using backward registration technique (Lin and Barron, 1994) according to the generated flow field. This flow determines the movement and becomes the ground-truth flow. The flow field determines the movement uniquely. Thus, it becomes the ground-truth flow field between these two frames and can be used for testing purposes. Owing to the property of the backward registration technique, the first frame represents the input real image before the movement while the second frame represents it after the movement. Therefore, the second frame is similar to the real input image. The generation process is illustrated in Fig. 1.

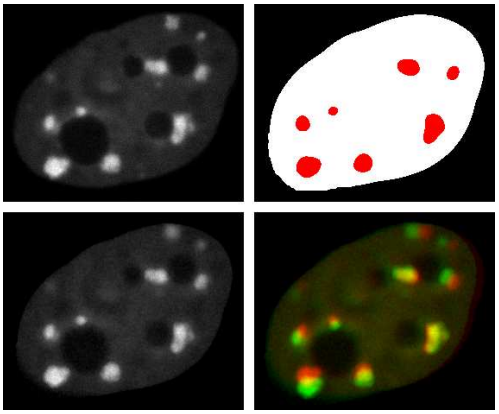

Figure 1: Generation of artificial data. We use two-layered approach. Both artificial frames are generated from the real input frame. The second frame is almost identical to the real one. The first frame is the backward registered copy of second frame. The artificial ground-truth flow field is used for the backward registration. The background and foreground movements are independent. **(top left).** Real input frame. **(top right)** Cell nucleus mask (background) in white, object mask (foreground) in red. **(bottom left)** Second artificial frame. **(bottom right)** First artificial frame (red channel) superimposed over second frame (green channel).

The first experiment was performed on artificial two dimensional data. We prepared a data set of artificial images with large local displacements. The data set consisted of six different frame couples. The size of input frames was 400×400 pixels. The number of objects which moved inside the nucleus varies from seven to eleven. The size of the individual translations vectors varies from 1.2 to 11.3 pixels. According to the literature, the input frames were filtered with gaussian blur filter with standard deviation $\sigma = 1.5$. We performed a parametric study over α parameter for four tested methods over whole data set. The results were compared with respect to average angular error (AAE) (Fleet and Jepson, 1990) where angular error is defined as

$$\arccos\left(\frac{(u_1)_{gt}(u_1)_e + (u_2)_{gt}(u_2)_e + 1}{\sqrt{((u_1)_{gt}^2 + (u_2)_{gt}^2 + 1)((u_1)_e^2 + (u_2)_e^2 + 1)}}\right) \tag{10}$$

where $(u_i)_{gt}$, $(u_i)_e$ denote the i-component of ground-truth and estimated vector, respectively. There were two coupled goals behind this experiment. We wanted to identify the best method by the mean of AAE and at the same time find suitable setting of α parameter. The results are presented in Fig. 2. The AAE was computed for each run of particular method with particular α. Then, the averages of AAE over the frame pairs in the data set were computed. These averages are depicted in the graphs in Fig. 2. The AAE was computed only inside the moving objects. We can see that all methods perform reasonably well. The CLG method is outperformed by the RDIA method. The gradient variant of CLG provided better results than the simple CLG method. The RDIA_G method is not depicted in the graph because we noticed that its results depended on data and the average value was biased. It was slightly better than simple RDIA method in some cases. But, it was slightly worse in other cases.

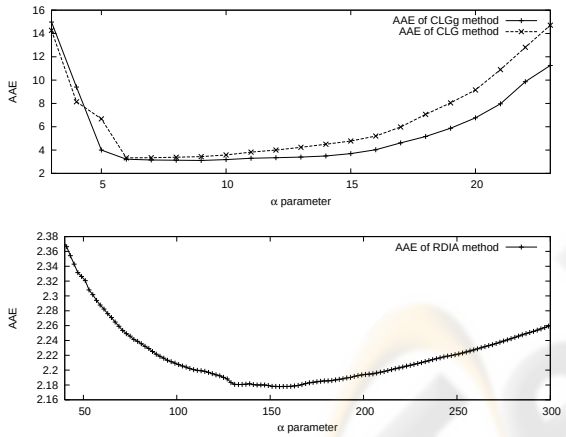

Figure 2: The dependency of average angular error on α parameter. The methods were tested on artificial image data with large local displacements up to 11.3 pixels. **(top).** CLG and CLG_G method. **(bottom)** RDIA method.

The goal of the second experiment was to examine the performance of the tested methods on sequences with combination of global and local movement. We again prepared a dataset with artificial frame pairs. Image size and other input sequence properties were the same as in the previous experiment. The cell nuclei were transformed with global translation (up to 5 pixels) and rotation (up to 4 degrees). After that the local displacement were applied on the foreground object inside. It becomes clear from our experiments that we should divide the data into two groups. The results of the computations were influenced by the following fact. If the majority of objects inside the cell nucleus moved in the direction similar to the

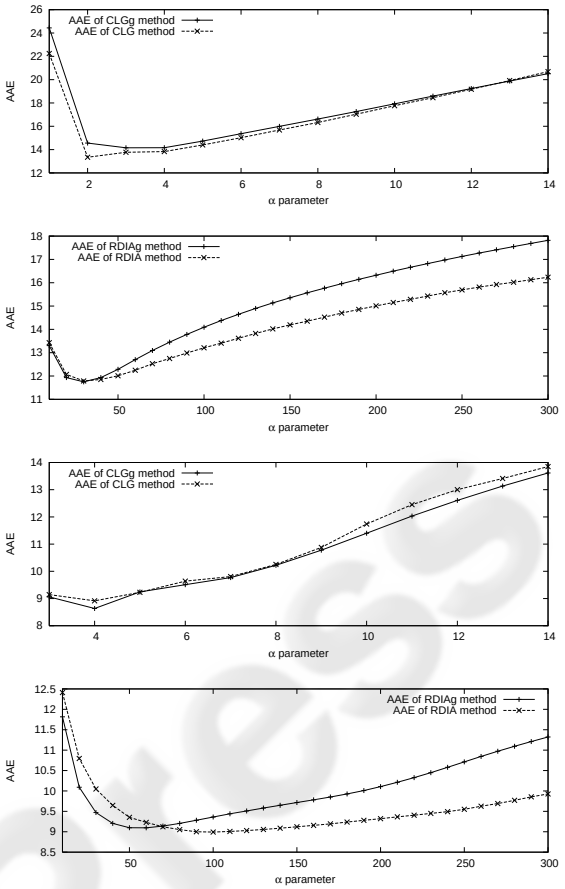

Figure 3: The dependency of average angular error on α parameter. The methods were tested on artificial image data with global movement (translation up to 5 pixels, rotation up to 4 degrees) and large local displacements up to 11.3 pixels. **(top).** CLG and CLG_G method. **(upper center)** RDIA and RDIA_G method. Majority of local displacements have the same direction as compared to global movement (top, upper center). **(lower center)** CLG and CLG_G method. **(bottom)** RDIA and RDIA_G method. Majority of local displacements has different direction than global movement (lower center, bottom).

global translation the results fell into the first group and vice versa. The AAE was computed on the cell nucleus mask (see the Fig. 1) in this experiment. The results for both groups are illustrated in Fig. 3.

We tested the methods with best parameter settings on real three dimensional data in the third experiment. We computed the displacement field of two input frames of human HL-60 cell nucleus with moving HP1 protein domains. There are global as well as local movements in the frame pair (see Fig. 4). We estimated the flow with RDIA method, α was set to 100. The size of the input frames was $276 \times 286 \times 106$. The results are illustrated in Fig. 4.

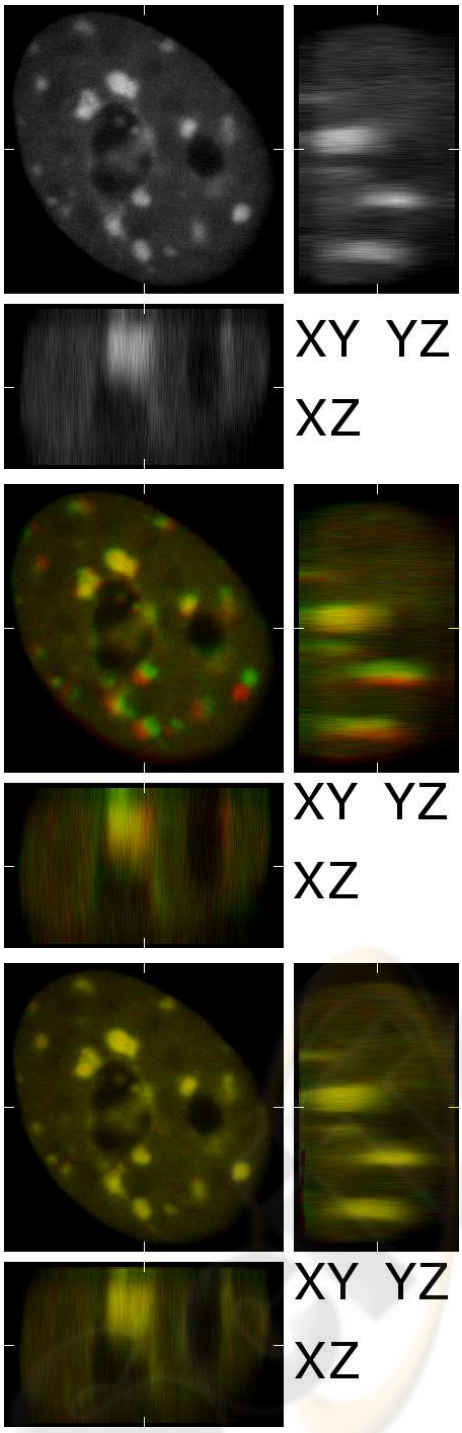

Figure 4: Experiment with real 3D data. Frame size $276 \times 286 \times 106$. *xy*, *xz* and *yz* cuts on position $(138, 143, 53)$ are shown. **(top).** First input frame. **(center)** First input frame (red channel) superimposed on second frame (green channel). Correlation is 0.901. **(bottom)** The RDIA method with $\alpha = 100$ computes the flow field. Backward registered second frame (green channel) is superimposed onto first frame (red channel). Correlation is 0.991.

The VOF methods were implemented in C++ language and tested on common workstation (Intel Pentium 4 2.6 GHz, 2 GB RAM, Linux 2.6.x). We use the multigrid framework (Bruhn, 2006) for numerical solution of tested VOF methods. The computations on two 3D frames of size $276 \times 286 \times 106$ took from 700 to 920 seconds and needed 1.5 GB of RAM. Computations on two 2D frames of size 400×400 took from 13 to 16 seconds and needed 13 MB of RAM.

3.1 Discussion

We found out that the RDIA methods produce slightly better results than the CLG methods (with respect to AAE) in both experiments on synthetic live-cell image data. Moreover, RDIA methods are less sensitive to α parameter setting. It became clear that the smoothing term of RDIA method is more suitable for the low contrast image sequences. The computed flow field can be easily oversmoothed by the CLG methods, because they consider the moving objects to be outliers in the data by particular parameter settings (larger α).

The use of "gradient" variants of tested method can slightly improve their performance on live-cell image data. On the other hand, there is no warranty that the result will be always better. Actually, the RDIA method seems to be more sensitive to α parameter when using its "gradient" variant. Surprisingly, the expected improvement of "gradient" variants was not significant even for fading out sequences. We suppose that the gradient constancy assumption does not help a lot, because the decrease of the intensities between two consecutive frames is not big. To sum it up, the 2D tests show that the RDIA method is the most suitable for our data. Therefore, we used it for the experiment on the 3D real image data. The backward registered results show perfect match on *xy*-planes. The match in *xz* and *yz* planes is a little bit worse. This is caused by the lower resolution of the microscope device in the *z* axis.

The bleeding-edge multigrid technique allowed us to get the flow fields in reasonable times even for 3D (up to 15 minutes for one frame pair). Small data sets which consist of only tens of frames of several cells can be analyzed in order of days on one common PC. Larger data sets as well as parametric studies in 3D should be analyzed on a computer cluster.

4 CONCLUSION

We studied state-of-the-art variational optical flow methods for large displacement for motion tracking

of fluorescently labeled targets in living cells. We focused on 2D as well as 3D images. Up to our best knowledge, we tested those methods first time in the literature for *three* dimensional image sequences.

We showed that these methods can reliably estimate large local divergent displacements up to ten pixels. Moreover, the methods can estimate the global as well as local movement simultaneously. The variants of CLG and RDIA method with gradient constancy assumptions did not bring significant improvement for our data. The RDIA method produced the best results in our experiments. We achieved reasonable computation times (even for three dimensional image sequences) using the full bidirectional multigrid numerical technique.

We plan to perform larger parametric studies on three dimensional data. This studies need to be performed on computer cluster or grid because of computational demands. Owing to the achieved results, we also feel confident in building a motion tracker as an application based on tested methods. By analyzing computed flow field one can extract important biological data regarding the movement of intracellular structures.

ACKNOWLEDGEMENTS

This work was partly supported by the Ministry of Education of the Czech Republic (Grants No. MSM-0021622419 and LC-535) and by Grant Agency of the Czech Republic (Grant No. GD102/05/H050).

REFERENCES

Barron, J. L., Fleet, D. J., and Beauchemin, S. S. (1994). Performance of optical flow techniques. *Int. J. Comput. Vision*, 12(1):43–77.

Briggs, W. L., Henson, V. E., and McCormick, S. F. (2000). *A multigrid tutorial: second edition*. Society for Industrial and Applied Mathematics, Philadelphia, PA, USA.

Bruhn, A. (2006). *Variational Optic Flow Computation: Accurate Modelling and Efficient Numerics*. PhD thesis, Department of Mathematics and Computer Science, Universität des Saarlandes, Saarbrücken.

Bruhn, A. and Weickert, J. (2005). Towards ultimate motion estimation: Combining highest accuracy with real-time performance. In *Proc. 10th International Conference on Computer Vision*, pages 749–755. IEEE Computer Society Press.

Bruhn, A., Weickert, J., and Schnörr, C. (2005). Variational optical flow computation in real time. *IEEE Transactions of Image Processing*, 14(5).

Chalfie, M., Tu, Y., Euskirchen, G., Ward, W. W., and Prasher, D. C. (1994). Green fluorescent protein as a marker for gene-expression. *Science*, 263(5148):802–805.

Dawood, M., Lang, N., Jiang, X., and Schäfers, K. P. (2005). Lung motion correction on respiratory gated 3d pet/ct images. *IEEE Transactions on Medical Imaging*.

de Leeuw, W. and van Liere, R. (2002). Bm3d: Motion estimation in time dependent volume data. In *Proceedings IEEE Visualization 2002*, pages 427–434. IEEE Computer Society Press.

Fleet, D. J. and Jepson, A. D. (1990). Computation of component image velocity from local phase information. *Int. J. Comput. Vision*, 5(1):77–104.

Gelfand, I. M. and Fomin, S. V. (2000). *Calculus of Variations*. Dover Publications.

Horn, B. K. P. and Schunck, B. G. (1981). Determining optical flow. *Artificial Intelligence*, 17:185–203.

Kozubek, M., Matula, P., Matula, P., and Kozubek, S. (2004). Automated acquisition and processing of multidimensional image data in confocal in vivo microscopy. *Microscopy Research and Technique*, 64:164–175.

Lin, T. and Barron, J. (1994). Image reconstruction error for optical flow. In *Vision Interface*, pages 73–80.

Manders, E. M. M., Visser, A., Koppen, A., de Leeuw, W., van Driel, R., Brakenhoff, G., and van Driel, R. (2003). Four-dimensional imaging of chromatin dynamics the assembly of the interphase nucleus. *Chromosome Research*, 11(5):537–547.

Matula, P., Matula, P., Kozubek, M., and Dvořák, V. (2006). Fast point-based 3-d alignment of live cells. *IEEE Transactions on Image Processing*, 15:2388–2396.

Nagel, H. H. and Enkelmann, W. (1986). An investigation of smoothness constraints for the estimation of displacement vector fields from image sequences. *IEEE Trans. Pattern Anal. Mach. Intell.*, 8(5):565–593.

Papenberg, N., Bruhn, A., Brox, T., Didas, S., and Weickert, J. (2006). Highly accurate optic flow computation with theoretically justified warping. *International Journal of Computer Vision*, 67(2):141–158.

Zitová, B. and Flusser, J. (2003). Image registration methods: a survey. 21(11):977–1000.